minerals

Article

Investigation of Internal Classification in Coarse Particle Flotation of Chalcopyrite Using the CoarseAIR™

Luke J. Crompton *, Md. Tariqul Islam and Kevin P. Galvin

ARC Centre of Excellence for Enabling Eco-Efficient Beneficiation of Minerals, Newcastle Institute for Energy and Resources, University of Newcastle, Callaghan, NSW 2308, Australia; tariqul.islam@newcastle.edu.au (M.T.I.); kevin.galvin@newcastle.edu.au (K.P.G.)
* Correspondence: luke.crompton@uon.edu.au

Abstract: This work introduces the CoarseAIR™, a novel system utilizing a three-phase fluidized bed and a system of inclined channels to facilitate coarse particle flotation and internal size classification. Internal classification in the CoarseAIR™ was investigated in a series of continuous steady-state experiments at different inclined channel spacings. For each experimental series, a low-grade chalcopyrite ore was milled to a top size of 0.53 mm and methodically prepared to generate a consistent feed. The air rate to the system was adjusted to determine the impact of the gas flux on coarse particle flotation and overall system performance, with a focus on maximizing both copper recovery and coarse gangue rejection. A new feed preparation protocol led to low variability in the state of the feed, and in turn strong closure in the material balance. Hence, clear conclusions were drawn due to the high-quality datasets. Inclined channel spacings of z = 6 and z = 9 mm were used. The z = 9 mm spacing produced more favourable copper recovery and gangue rejection. Higher gas fluxes of 0.30 to 0.45 cm/s had a measurable, adverse effect on the recovery of the coarser hydrophobic particles, while the gas flux of 0.15 cm/s delivered the best performance. Here, the cumulative recovery was 90%, and mass rejection was 60% at 0.50 mm, while the +0.090 mm recovery was 83% with a gangue rejection of 85%. The system displayed robust performance across all conditions investigated.

Keywords: coarse particle flotation; CoarseAIR; early gangue rejection; fluidisation; fluidization; chalcopyrite; flotation

Citation: Crompton, L.J.; Islam, M.T.; Galvin, K.P. Investigation of Internal Classification in Coarse Particle Flotation of Chalcopyrite Using the CoarseAIR™. *Minerals* **2022**, *12*, 783. https://doi.org/10.3390/min12060783

Academic Editor: Thomas Mütze

Received: 20 May 2022
Accepted: 16 June 2022
Published: 20 June 2022

1. Introduction

Froth flotation is arguably one of the greatest innovations of the 20th century [1]. Challenges remain, however, especially in recovering ultrafine and coarse particles [2]. At the ultrafine sizes below about 20 µm [3], viscous lubrication forces impede the particle–bubble collision, preventing adhesion, while at the coarser sizes beyond 100 µm the particles readily adhere, but then detach, especially within the turbulent flow field of a mechanical flotation cell. Coarse particles also exhibit lower levels of surface liberation, further reducing the probability of coarse particle–bubble attachment and hence recovery [4]. Indeed, conventional flotation technologies have proven to be highly inefficient in achieving coarse particle flotation, requiring long residence times, and hence a large footprint, while requiring considerable energy input to maintain their suspension in the flotation cell [5]. An increasing number of studies have shown that the provision of a quiescent, fluidized bed environment provides sufficient opportunity for achieving bubble–particle adhesion while offering protection from particle–bubble detachment forces [6–8].

The grades of ore bodies across most commodities are in decline, with chalcopyrite grades invariably lower than 1 wt% copper. The hard rock must undergo crushing and grinding to a size sufficient for achieving concentration and recovery. The conventional approach has been almost one-dimensional, literally grinding the entire ore body to a grind size with a P_{80} of 75 μm, and even finer. Napier-Munn [9] has estimated that up to 2% of global electrical energy is consumed through comminution, while Ballantyne and Powell [10] have estimated that up to 1.3% of Australia's electrical energy is consumed through comminution of gold and copper ores alone. Hence, with the current drive towards net-zero emissions, there are major incentives to reduce the extent of the comminution. Many mining operations are in arid regions; thus, water consumption is also a major concern. The fine grinding creates excessive quantities of ultrafine particles below 20 μm, greatly limiting water recovery, while also making tailings storage more costly, and problematic. This problem can, in part, be addressed by reducing the degree of fine grinding.

Coarse particle flotation has been gaining increasing traction within the industry, motivated by the need to reduce energy and water consumption in minerals processing. Low-grade ores are subjected to comminution to release the valuable minerals; more importantly, the lower-value gangue minerals can be rejected from the process circuit, ideally at the largest particle size. By maximizing the particle size of the gangue minerals, it follows that the energy consumption associated with the grinding is minimized, given the gangue minerals constitute most of the ore body mass [11]. Similarly, this approach leads to high water recovery.

As alluded to already, froth flotation of mineral particles is effective over only a limited particle size ranging typically from 10 to 100 μm. At particle sizes above 100 μm, gravity separation is commonly applied to process these coarser particles; however, for low-grade ores, the density of a coarse particle containing a dense mineral is often only marginally higher than that of the low-value gangue mineral. In recent years, there has been a convergence of the previously distinct fields of gravity separation and flotation, utilizing the quiescent properties of the fluidized bed to promote the flotation of these coarse particles. To introduce coarse particle flotation, Eriez has developed the HydroFloat cell, which consists of an upward current fluidized bed, similar to the Teetered Bed Separator, with air supplied to the system to generate fine bubbles that rise up through the fluidized suspension [12,13]. The air bubbles intercept hydrophobic particles, achieving adhesion, and in turn transporting those particles upwards to the overflow.

The bulk of the volumetric feed flow to the HydroFloat reports to the overflow. This means the system operates like a classifier, with particles finer than the classification size partitioning to the overflow, with the coarse hydrophobic particles attached to rising air bubbles. Thus, the recovery of the valuable minerals should be almost complete provided they are finer than the classification size. The challenge is to ensure that the hydrophobic particles larger than the classification size are also recovered to the overflow.

In practice, the feed to the HydroFloat is prepared using a fluidized bed classifier to produce a relatively dilute stream of overflow fines less than 100 μm in size, ideal for conventional flotation. The underflow from the classifier consisting of the relatively coarse particles, larger than 100 μm [12], is sent to the HydroFloat. This pre-classification greatly increases the footprint and capital cost of the installation. Moreover, it must be achieved with high levels of efficiency, precluding the use of cheaper hydrocyclones. The approach does, however, ensure the overflow product from the HydroFloat achieves a strong upgrade, ideal for further comminution. In turn, the underflow from the HydroFloat provides a basis for rejecting coarse gangue from the circuit.

Another coarse particle flotation technology is the Nova Cell, which also introduces air bubbles into a fluidized bed system [14]; however, here an intermediate stream is generated. This intermediate stream reduces the overflow liquid flux, enabling a froth to emerge from the cell. The intermediate stream captures relatively coarse hydrophobic particles that fail to join the froth, along with finer gangue minerals. This stream must be directed to a further classifier to recover and concentrate the coarse particles. Assuming the froth recovery of the fines is highly efficient, this intermediate stream can be classified using a relatively inefficient cyclone, producing a coarse stream ideal for further comminution. The underflow from the Nova Cell also provides a basis for rejecting coarse gangue from the circuit, together with the more dilute overflow from the cyclone.

The present study was concerned with a third coarse particle flotation device, known as the CoarseAIR™, shown in Figure 1. This device is derived from the REFLUX™ Classifier, which consists of a lower fluidized bed, and an upper system of inclined channels. Air is introduced into the fluidization water to form fine air bubbles that rise upwards with the water, through the fluidized bed. The feed suspension, delivered at an intermediate elevation, flows upwards into the system of inclined channels, while coarser particles plummet into the lower fluidized bed.

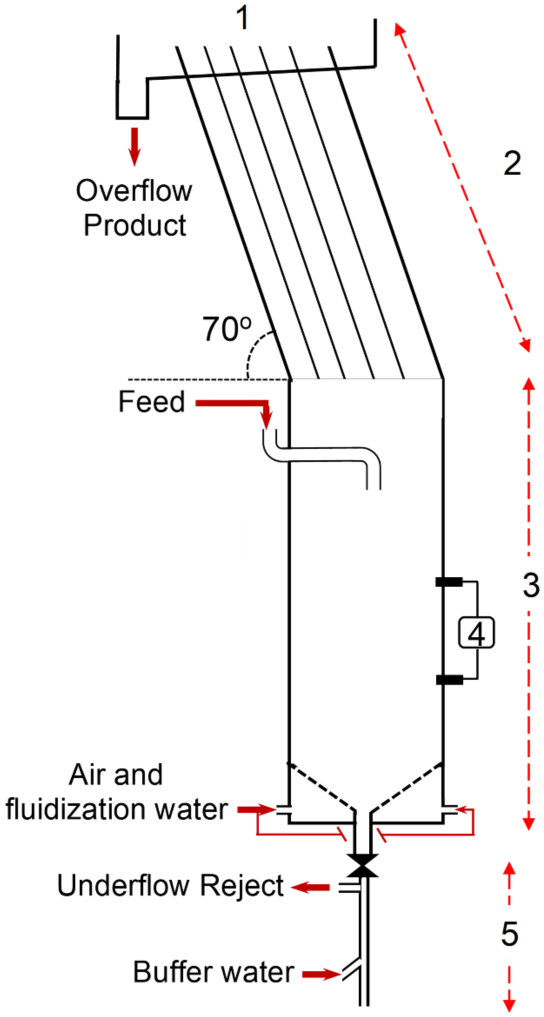

Figure 1. Schematic view of the CoarseAIR™. (1) Overflow launder, (2) inclined channels, (3) vertical fluidized bed column, (4) differential pressure sensor, (5) buffer system to moderate underflow discharge.

It is well-known that the REFLUX™ Classifier is a powerful classifier due to the so-called Boycott effect [15]. Particles segregate onto the upward-facing surfaces of the inclined channels before returning to the lower zone while the finer particles continue to convey upwards. Here, hydrophobic particles that settle into the lower zone attach to the rising air bubbles, and in turn convey upwards through the system of inclined channels, into the overflow. Thus, the hydrophobic particles and the entrained hydrophilic particles report together with the overflow. These can be separated via an inefficient hydrocyclone allowing the coarse portion to undergo final comminution, while the fine portion undergoes flotation. Again, the relatively coarse gangue minerals discharge via the underflow stream.

Clearly, the internal classification of the CoarseAIR™, utilizing a system of inclined channels, represents a significant shift in the system hydrodynamics from that of both the HydroFloat and the Nova Cell. This internal classification replaces the need for an efficient upfront classifier, as required for the HydroFloat, enhancing fine particle gangue rejection directly to the underflow. This device does not seek to produce a concentrate, as occurs in the Nova Cell. Rather, the goal is to ensure the highest possible recovery of hydrophobic particles is achieved, utilizing the entrainment mechanism to deliver very close to 100% capture of the very finest particles. This approach then permits the most effective system of flotation to be applied to the overflow stream. The smaller coarse portion of the overflow is then subjected to further grinding.

The purpose of the present study was to investigate the internal classification of the CoarseAIR™ system in the context of coarse particle flotation. In gravity separation, the inclined channel perpendicular spacing, z, is usually set at 6 mm, but increasingly has been set at 3 mm, and even as narrow as 1.8 mm, to exploit shear-induced inertial lift, and hence upwards transport of lower-density particles. It is known, however, that particle size classification is promoted using wider channels; hence, for the present work the channel spacing was set at 6 mm and 9 mm in separate series of experiments. The effects of the gas flux and hence the bubble–particle transport were also investigated for each of these channel spacings. All the experiments involved a low-grade chalcopyrite feed, freshly ground, and supplied to the CoarseAIR™, with the system operated under continuous steady-state conditions. The system performance was assessed as a function of the particle size in terms of the solids and copper partitioning to the overflow. The goal was to maximize copper recovery and coarse gangue rejection.

2. Experimental Section

Experiments were conducted using a laboratory-scale CoarseAIR™ system, shown schematically in Figure 1. The system consisted of a vertical fluidized bed section, 1.5 m high with a 0.1 m $\times$ 0.1 m cross-sectional area. Fluidization water entered via a plenum chamber together with air, forming a flow of fine bubbles distributed via a series of nozzles located across the distributor. The upper portion of the system consisted of a series of channels, inclined at 70° to the horizontal. The feed entered the system via an inlet 0.2 m below the inclined channels. In these experiments, the feed consisted of a low-grade chalcopyrite ore, nominally finer than 0.50 mm. An autogenous fluidized bed developed in the lower part of the system, while a more dilute zone formed above. The entering feed suspension tended to flow upwards via the system of inclined channels, while coarser particles settled and joined the lower bed. At steady state, a relatively coarse underflow discharged from the system at a rate governed by a peristaltic pump, informed by the suspension density and the level of the fluidized bed. The product overflow stream emerged from the overflow launder.

2.1. Feed Preparation

For each experimental program, a 250 kg sample of low-grade chalcopyrite ore with a top size of approximately 20 mm was crushed using a laboratory jaw crusher to a top size of 3 mm. This material was then washed over a Kason vibratory screen to prevent the overgrinding of fines generated during crushing. The oversized material was then fed to a laboratory rod mill to pass through a 0.53 mm screen.

One of the major challenges associated with experimental investigation of coarse particle flotation is in delivering a consistent feed suspension containing a relatively wide size distribution of particles. It is important to recognize that it is impossible to form a homogenous suspension of particles in a tank, especially for dense particles with a size range of several hundred microns. The basic goal of a mixing tank is to ensure all solids are re-suspended off the bottom of the tank. In earlier work, we used a powerful stirrer, baffles, and four impellors on the one shaft. We also used a centrifugal pump to withdraw the slurry from the base of the tank at ~100 L/min to create a flow loop that returned the slurry to a higher level in the tank. Feed to the CoarseAIR™ was then withdrawn from the flow loop using a peristaltic pump. In this earlier work, it was discovered that the feed underwent changes with time due to the cumulative effects of particle segregation within the feed tank, and changes in mixing intensity within the feed tank as the feed volume decreased. The variable nature of the feed, covering short and longer time scales, created internal dynamic variations in the underflow and overflow throughout the experiment. These variations made it difficult to form clear conclusions from the early series of experiments. We believe that these issues have plagued other similar studies in the past.

A new method of feed preparation was therefore introduced to this work. The approach consisted of an initial phase of feed preparation using a relatively large tank. After milling, the ore was transferred to a 1300 L mixing tank and diluted to the desired pulp density. The resultant slurry was then conditioned with the collector, promoter, and the frother. After conditioning, the feed was evenly distributed sequentially into approximately one hundred 20 L buckets, each containing about 12 L of slurry, with pulp density ranging from 20 to 25% solids. This sequence of buckets was then randomized, using a random number generator, before being fed sequentially into a 300 L mixing tank, along with water conditioned with frother to dilute the slurry to the required feed pulp density.

2.2. Continuous Steady-State Operation

As previously noted, it is almost impossible to produce a homogeneous suspension in a mixing tank. It is best to treat the mixing tank as a process vessel that is subject to particle segregation. Then, if there is one input to the tank, and a fixed output, ultimately the inputs equal the outputs. Here, the 300 L stirred tank offered a degree of buffering against naturally occurring discrepancies in the compositions of each added bucket of feed. Buckets of feed were added to the feed tank at a rate sufficient to maintain a consistent level in the tank. Once a sufficient period had passed, typically about an hour (or the addition of 20 buckets of the feed), the output from the tank was deemed to be constant. This consistency of the feed to the CoarseAIR™ is illustrated below in Figure 2, which shows the particle size distribution of three feed samples collected over the course of a 5 h experiment, displaying minimal variation across the samples. It should be appreciated that the maintenance of this level of consistency over such a long period of time is extraordinary and is now the subject of a separate formal study within our group. It is further noted that the delivery of this consistent feed resulted in consistent output streams from the CoarseAIR™, with almost no need for undertaking mass balance reconciliation.

Once the feed suspension was added to the CoarseAIR™, and the fluidization water and gas flux were applied, the system evolved towards a steady-state separation. The underflow rate was adjusted to establish a constant bed level in the system. It is noted that an underflow buffer, described previously [16], was applied to help moderate the underflow removal. Buffer water was applied at a rate of 1.0 L/min, less than the rate of underflow removal; thus, there was no net buffer water flow into the system. The fluidization rate was adjusted to ensure a satisfactory bed density within the CoarseAIR™. This suspension density was measured using two pressure transducers located 50 mm and 300 mm above the base of the distributor. The fluidization rate produced a density consistent with a volume fraction of solids of order 0.45. Bed height was maintained through adjustment of the underflow rate; however, it is noted that the uniform feed condition resulted in the need for little or no adjustment to the underflow rate at any time.

2.3. Coarse Particle Sampling

A screen with a sieve aperture of 0.355 mm was located for set time intervals under the overflow stream to measure the rate of capture of the coarsest overflow particles. These samples provided a sensitive real-time measure of the coarse particle flotation. Careful wet screening of these samples was important to ensure the measured mass was accurate. Changes in the gas flux resulted in changes in the capture rates of these particles.

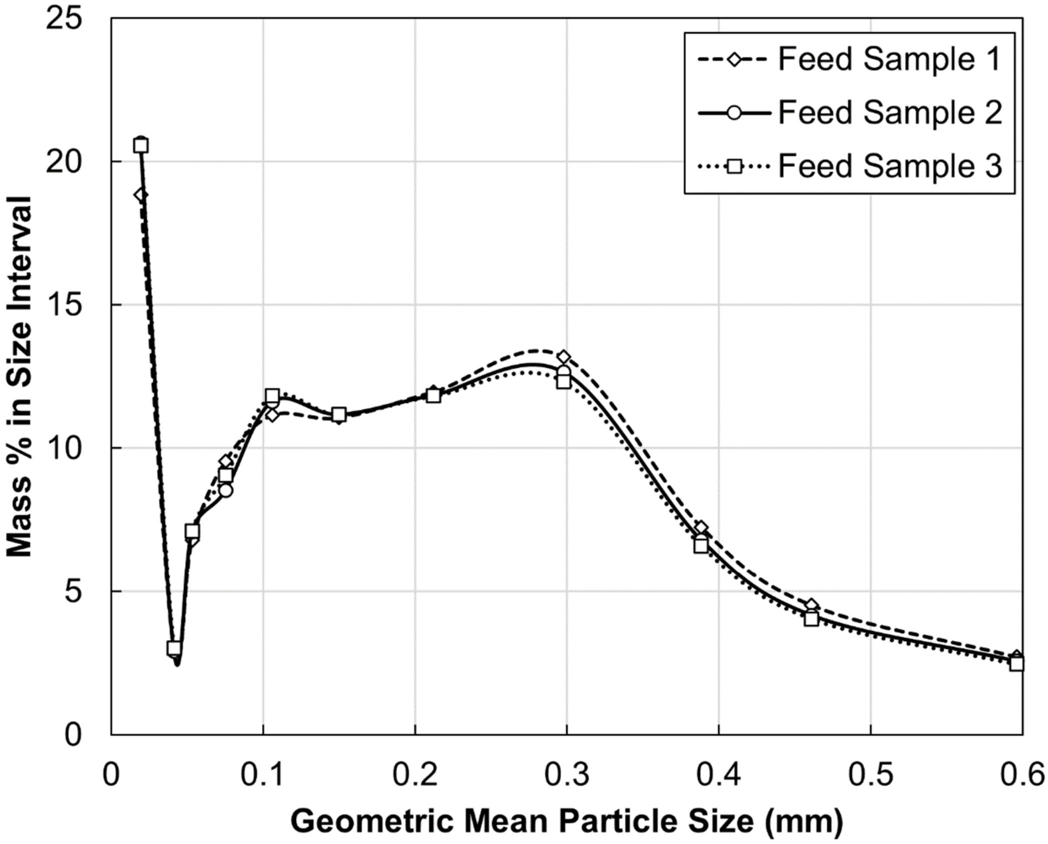

Figure 2. Feed samples taken during one experiment. Feed samples were collected at approximately 90 min, 210 min, and 250 min run time, respectively. The size distributions of the feed samples are almost identical.

2.4. Steady-State Sampling

Once the system was deemed to have reached steady state, simultaneous samples of the underflow and overflow were taken. Typically, each stream was sampled for a period of 12 min. There was no valve closure; hence, the underflow discharge was very consistent. Once these samples had been taken, the feed to the system was diverted so that a feed sample could also be obtained. Sometimes back-to-back experiments were conducted, greatly reducing the overall run times required to reach steady state. In these experiments, the feed to the CoarseAIR™ was resumed once the feed sample had been taken.

2.5. Summary of Experimental Conditions

Experimental parameters for each set of tested conditions are outlined in Table 1. Reagent dosages were consistent throughout the experimental program and consisted of Aero MX and sodium isobutyl xanthate (SIBX) as promoter and collector, respectively. Methyl isobutyl carbinol (MIBC) and Matfroth-50 were used as frothers, with lime used to modify pH. The dosage of reagents and conditioning time during the feed preparation are shown in Table 2.

Table 1. Parameters for each experiment.

Experiment ID (-)	Channel Spacing, z (mm)	Pulp Density (wt%)	Feed Flux(cm/s)	Fluidization Water (cm/s)	Gas Flux (cm/s)	Solids Throughput (t/(m^2·h))
1-A	6	9.9	1.29	0.22	0.30	4.2
1-B	6	9.3	1.27	0.22	0.15	3.8
1-C	6	9.7	1.25	0.22	0.45	3.9
1-D	6	9.1	1.27	0.22	0.075	3.7
1-E	6	9.4	1.26	0.22	0.03	3.8
1-F	6	9.1	1.26	0.22	0.15	3.7
2-A	9	9.6	1.25	0.22	0.30	3.8
2-B	9	10.2	1.24	0.22	0.075	4.1
2-C	9	10.0	1.25	0.22	0.45	4.0
2-D	9	10.1	1.25	0.22	0.15	4.1
2-E	9	9.5	1.26	0.22	0.30	3.8

Table 2. Reagents and conditioning time used during experiments.

Reagents	Purpose	Dosage	Time (min)
Aero MX	Promotor	15.65 mL/t of Cu ore	5
Sodium isobutyl xanthate (SIBX)	Collector	72 g/t of Cu ore	5
Methyl isobutyl carbinol (MIBC)	Frother	25.4 ppm	5
Matfroth-50	Frother	3.9 ppm	5

3. Results and Discussion

The experimental program was concerned with the internal classification of the particles within the CoarseAIR™. One series of experiments was conducted using an inclined channel spacing of z = 6 mm, and a second with z = 9 mm. Previous work on gravity separation in the REFLUX™ Classifier has been enhanced through use of closely spaced inclined channels with z = 6 mm, and more recently z = 3 and z = 1.8 mm. These closely spaced inclined channels promote inertial lift and hence particle transport of relatively low-density particles to the overflow. The shear-induced inertial lift declines rapidly as the channel spacing increases. Thus, particle size classification is expected to be strongly favoured by the wider channel spacing of z = 9 mm, in turn releasing more of the solids to the underflow.

The work in this paper was focussed on relatively low solids throughputs of ~4 t/(m^2·h). The low throughputs permitted a more significant range of experimental conditions to be covered for a given quantity of the prepared feed. The low throughput also helped to build a stronger focus on the internal classification. The plan is to investigate the effects of increasing solids throughputs in future studies. The low throughput also permitted a series of low gas fluxes to be used in an extended series of experiments, with several different gas fluxes introduced as step changes to provide clear evidence on any shift in performance due to the gas flux. In future experiments involving higher throughputs, it will be necessary to establish whether these findings continue to apply.

3.1. Error Analysis

In an ideal steady-state process, the amount of mass entering the system equals the amount of mass exiting the system. Similarly, with no chemical reactions or particle size reduction, the mass of copper and total mass within a set particle size interval entering the system must equal the mass in that interval exiting the system. In practice, this condition is rarely met due to systematic and random errors incurred during measurement and sampling.

The new protocol established to deliver the feed to the CoarseAIR™ led to very consistent results. Table A1 shows the size distributions and assay values of the feed, product, and reject streams from two experiments, comparing the raw data and the corresponding data following mass balance reconciliation [17]. Figure 3 below shows an example of a log–log plot of the raw and balanced grade and size distribution data for Experiment 2-C. It is noteworthy that this experiment had the highest amount of relative error between experimental and mass balanced sizing values for this series of experiments. It is clear the data adjustment required to achieve a mass balance involved minimal adjustments, the standard deviation in the adjustment or error being only 5% for copper assays. For the size distributions, the adjustments were also relatively small with a standard deviation in the adjustments or error of only 11%. A Monte Carlo simulation technique was applied to these errors in the assay values to determine the corresponding standard deviation in the yields and recoveries by size, and cumulative yields and recoveries for each data set. Error bars shown in the following graphs represent a confidence interval of 95%.

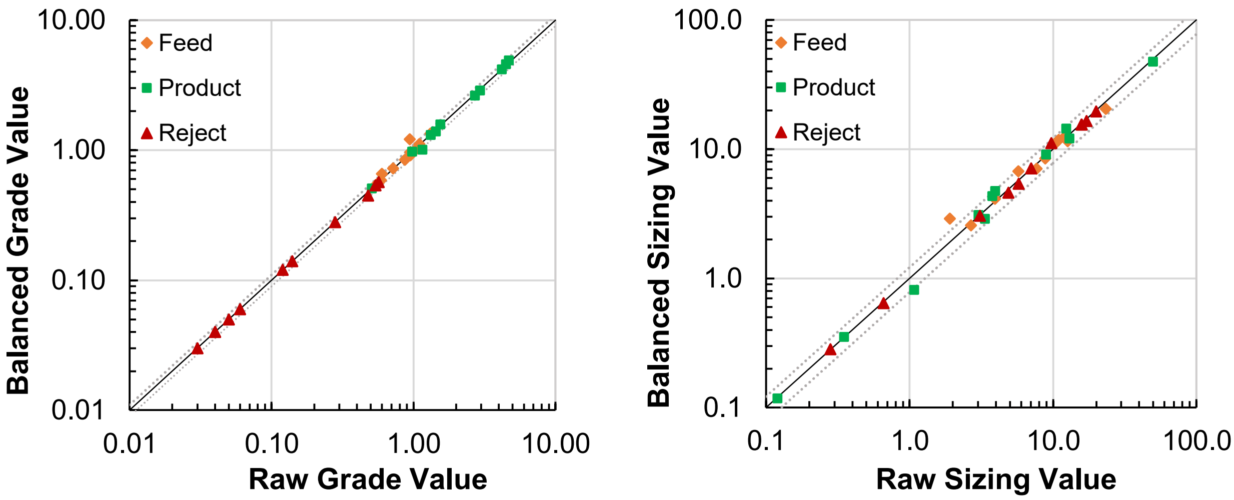

Figure 3. Log–log plot comparing experimental and mass balanced values from Experiment 2-C (0.45 cm/s, z = 9 mm). The dotted lines represent a 95% confidence interval.

3.2. Particle Classification in the CoarseAIR™

Figure 4 shows the solids partition numbers versus the particle size for the z = 6 mm and the z = 9 mm inclined channels. Four cases are shown covering gas fluxes of (a) 0.075 cm/s, (b) 0.15 cm/s, (c) 0.30 cm/s, and (d) 0.45 cm/s. The graphs show the probability of a particle of a given size reporting to the overflow. The partition number to overflow was close to 1.0 at ultrafine sizes, decreasing rapidly to about 0.5 at particle sizes typically finer than 0.1 mm. In general, the 0.5 partition was reached at a finer size using the channel spacing of z = 9 mm. Thus, the classification was coarser using the 6 mm channels, and in fact became increasingly coarse as the gas flux increases. These results suggest the fluidized sands are more readily transported to the overflow in the 6 mm channels. The clear conclusion, therefore, is that the 9 mm channel spacing is more effective in rejecting the gangue particles. Moreover, the wider channel spacing should accommodate higher solids throughputs.

At coarser sizes, the partition curve does not rapidly drop to zero, but rather declines slowly, maintaining a significant finite portion that reports to the overflow even for sizes as large as 0.60 mm. These particles are too large to be easily entrained so must be reporting to the overflow due to their hydrophobicity, and hence are a manifestation of coarse particle flotation. At low gas fluxes, the hydrophobic coarse particle recovery is marginally higher in the 6 mm channels, but this situation gradually shifts as the gas flux increases, with the coarse particle recovery ultimately higher in the 9 mm channels. Overall, the proportion recovered clearly declines as the particle size increases, reflecting the increased difficulty in recovering coarser particles due to both their larger mass and decreasing surface liberation. Given the improved particle classification achieved in the wider channels, and hence the improved prospects for higher solids throughputs and gas fluxes, the focus of the study moved to the cases involving a channel spacing of z = 9 mm. These findings are extremely valuable moving forward, as higher gas fluxes may prove necessary at higher solids throughputs in future experiments.

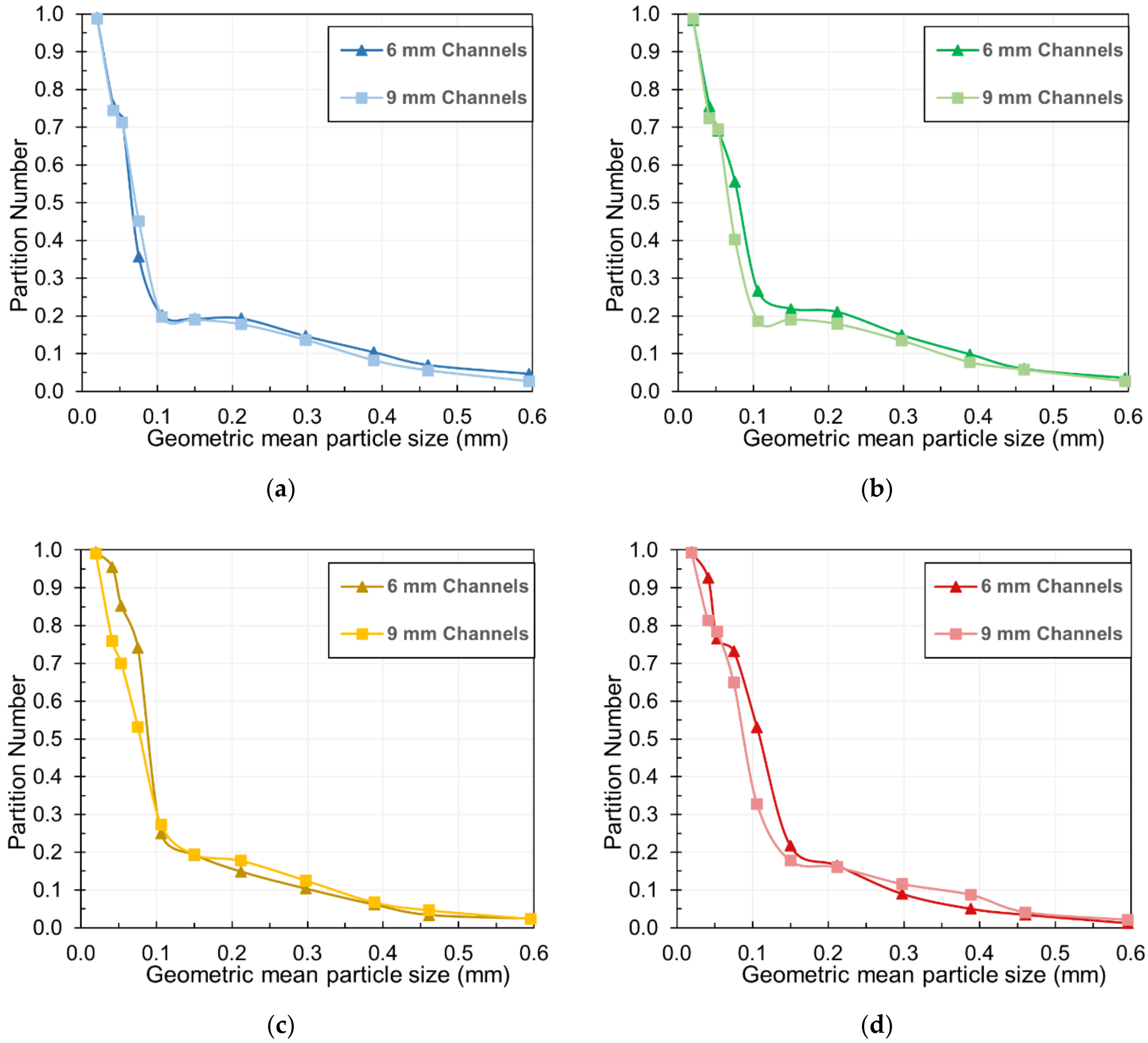

Figure 4. Partition-to-overflow product with 6 mm and 9 mm inclined channel spacings for four different sets of gas fluxes at (**a**) 0.075 cm/s, (**b**) 0.15 cm/s, (**c**) 0.3 cm/s, and (**d**) 0.45 cm/s.

3.3. The Effect of Gas Flux on Coarse Particle Flotation

A 0.355 mm screen was placed under the overflow from the CoarseAIR™ to capture the relatively coarse hydrophobic particles in timed intervals, typically every 5 min. This sampling during the experiment provided a valuable and sensitive measure of the coarse particle flotation and proved effective in assessing the impact of the gas flux on the flotation of coarse particles. The results are shown in Figure 5. The sequence of imposed gas fluxes was deliberately ad hoc to eliminate the effects of bias and any long-term trends. In fact, the sequence returned to the original gas flux of 0.30 cm/s at the end of the experiment.

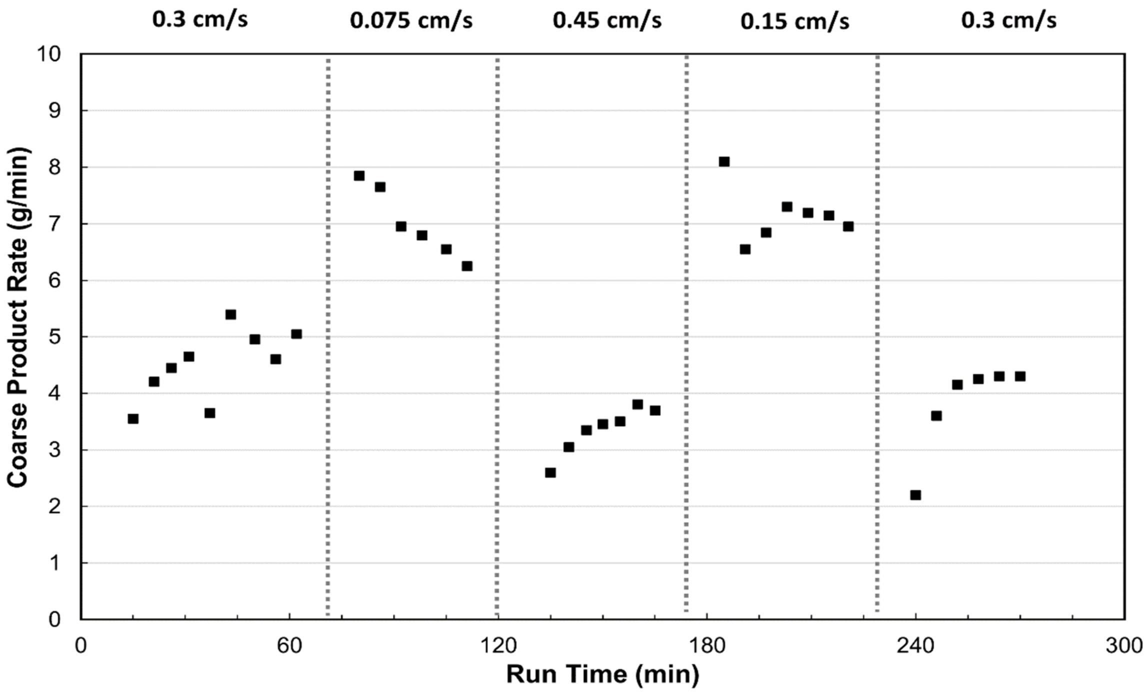

Figure 5. Measured coarse (+0.355 mm) product rate as a function of experiment run time. Dotted vertical lines indicate a change in the supplied gas rate, with the gas rate during each interval listed above.

It is evident the coarse particle flotation exhibited an intermediate level of performance at a gas flux of 0.30 cm/s, improved performance at a lower gas flux of 0.075 and 0.15 cm/s, and relatively poor performance at 0.45 cm/s. A noticeable feature is the sharp increase in the rate of coarse particle flotation soon after reducing the gas flux, evident at the beginning of the 0.075 and 0.15 cm/s increments, and a corresponding dip in the coarse particle flotation rate after increasing the gas flux. The coarse particle flotation rate took at least 20–30 min to recover from the step change in the gas flux.

It is unclear why there should be such a strong negative effect of increased gas flux on the coarse particle recovery. Perhaps the higher gas flux creates more disruption within the fluidized bed, and hence a less quiescent hydrodynamic state. It is noted that these samples only apply to the tail end of the size distribution where surface liberation is more limited, and hence particle recovery is more sensitive. Increasing bubble hold-up within the fluidized bed might lead to an increase in bubble coalescence, and hence the formation of larger, less effective bubbles rising through the bed. A higher gas flux may also lead to coalescence within the inclined channels and in turn particle detachment. It will be interesting to establish whether these trends continue to hold at higher solids throughputs in future studies.

3.4. Recovery of Copper

A comprehensive analysis was conducted on two of the experiments conducted using the z = 9 mm channel spacing. The analysis was conducted on the highest performing experiment involving a gas flux of 0.15 cm/s and the poorest performing experiment involving a gas flux of 0.45 cm/s, thus providing the strongest possible contrast. For the experiments conducted at the other gas fluxes, assays were performed on the overflow product and underflow reject streams, and additional analysis was conducted on the assays above and below 0.090 mm. This particle size of 0.090 mm provided a useful basis for differentiating between the coarse particle flotation, and the recovery at the finer sizes.

The effect of the gas flux on copper recovery in the overflow product is shown in Figure 6. For the −0.090 mm overflow product, the copper recovery exceeded 99% in every case. This near complete recovery of the −0.090 mm portion reflects the strong effects of entrainment at ultrafine sizes and ensures the overflow can be confidently processed using fit-for-purpose highly efficient flotation cells, designed to maximize recovery. For the +0.090 mm overflow, the highest recovery was 83% at a gas flux of 0.15 cm/s, corresponding to an overflow mass yield of 14.7% (Figure 7), and hence a gangue rejection of 85.3%. These results help to further confirm the best overall performance was achieved at a gas flux of 0.15 cm/s, and poorer performance at 0.45 cm/s.

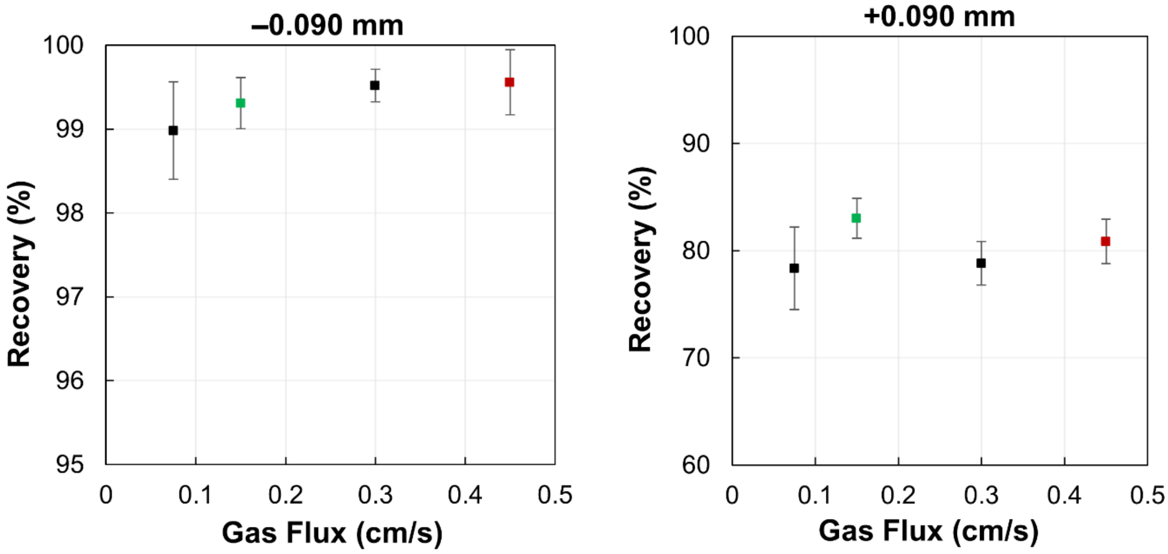

(**a**) (**b**)

Figure 6. Copper recovery in overflow product as a function of gas flux, split into a fine fraction passing through a screen with sieve aperture of 0.090 mm (**a**) and coarse fraction of +0.090 mm (**b**). Error bars show 95% confidence.

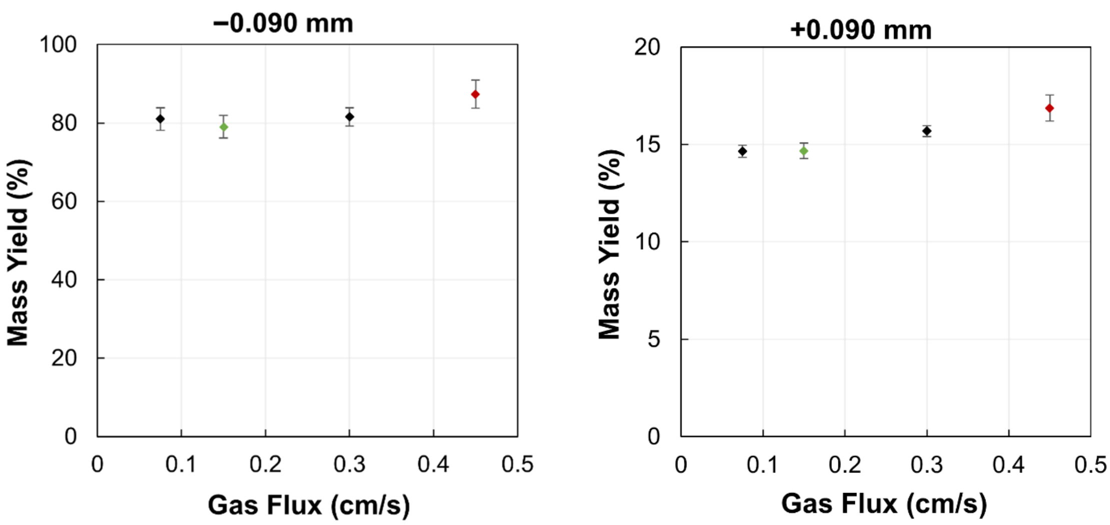

(**a**) (**b**)

Figure 7. Mass yield-to-overflow product as a function of gas flux for the particles passing through a screen with sieve aperture of 0.090 mm (**a**) and +0.090 mm particles (**b**) with the best (green) and poorest (red) performances highlighted. Error bars show 95% confidence.

The partitions-to-overflow product for the best (0.15 cm/s) and poorest (0.45 cm/s) performing gas fluxes are shown in Figure 8, together with the copper recovery as a function of particle size. A summary of mass balance data for these gas fluxes is given in Appendix A. The highest recovery was maintained across the entire size range using the lower gas flux of 0.15 cm/s. Importantly, this higher recovery was achieved at a higher level of coarse particle gangue rejection.

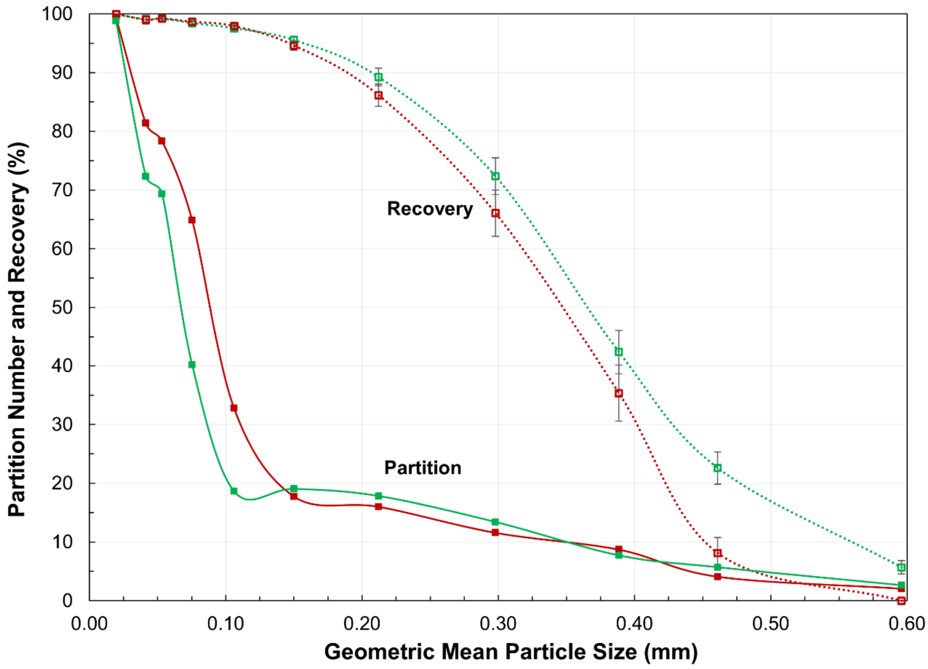

Figure 8. Partition-to-overflow product (filled squares and solid line) and copper recovery by size (unfilled squares and dotted line) for the best (green) and poorer (red) performing gas fluxes. Best performance had a gas flux of 0.15 cm/s, and poorer performance had a gas flux of 0.45 cm/s.

This overall condition is shown more clearly in Figure 9 in terms of the cumulative yield and the cumulative recovery of copper. At a gas flux of 0.15 cm/s, the cumulative recovery at a particle size of 0.50 mm was 90%, the cumulative yield was 40%, and hence the mass rejection was 60%. Cumulative recovery remained consistently high despite the lower mass yields for the lower gas flux case. The poorest result produced a cumulative recovery of 87.5%, yield of 44%, and hence mass rejection of 56%. This work confirms robust separation performance with the difference in performance across the work being relatively modest, but nevertheless significant. Clearly, there exists an optimum gas flux, which for this work was 0.15 cm/s.

Figure 10 shows the upgrade achieved at both the lower gas flux of 0.15 cm/s and the higher gas flux of 0.45 cm/s. At the finer particle sizes, the strong entrainment led to a relatively low product grade. However, as the particle size increased, the entrainment contribution declined appreciably, leading to higher product grades. At the coarsest sizes, the grade declined again due to the poorer surface liberation. The curves passing through the data are provided to guide the eye. Interestingly, the two cases show a common peak; however, the upgrades fell away more rapidly at both coarser and finer particle sizes for the higher gas flux.

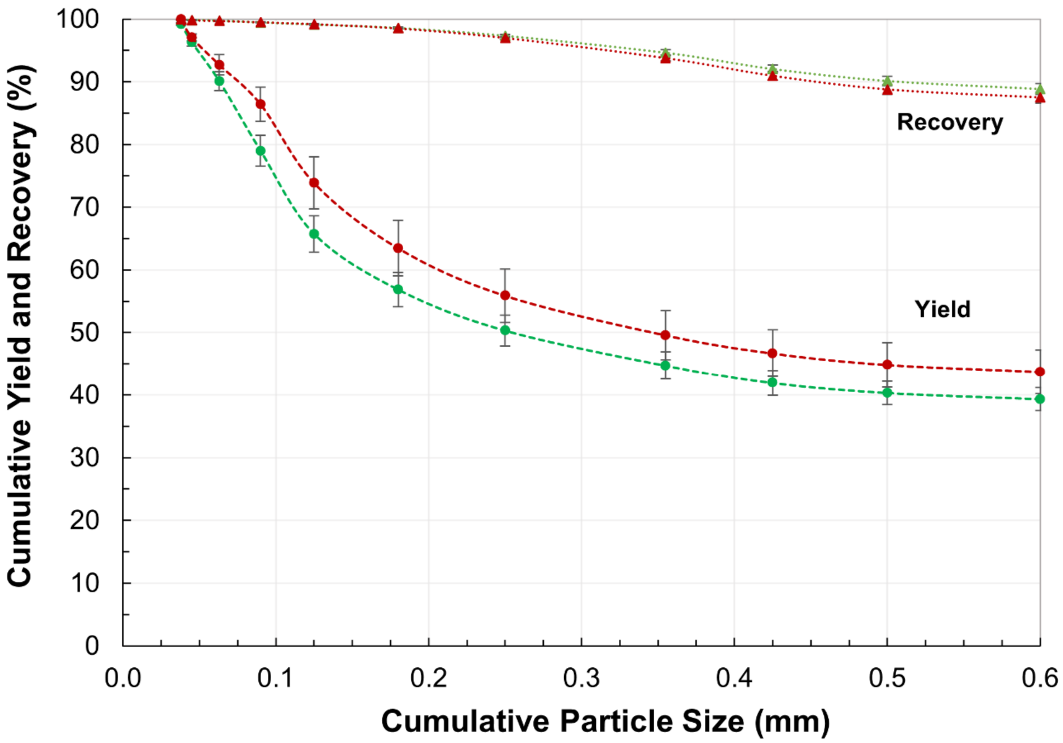

Figure 9. Cumulative yield (circles and broken line) and cumulative recovery (triangles and dotted line) for the best (green) and poorer (red) performing gas fluxes. Best performance had a gas flux of 0.15 cm/s and poorer performance had a gas flux of 0.45 cm/s.

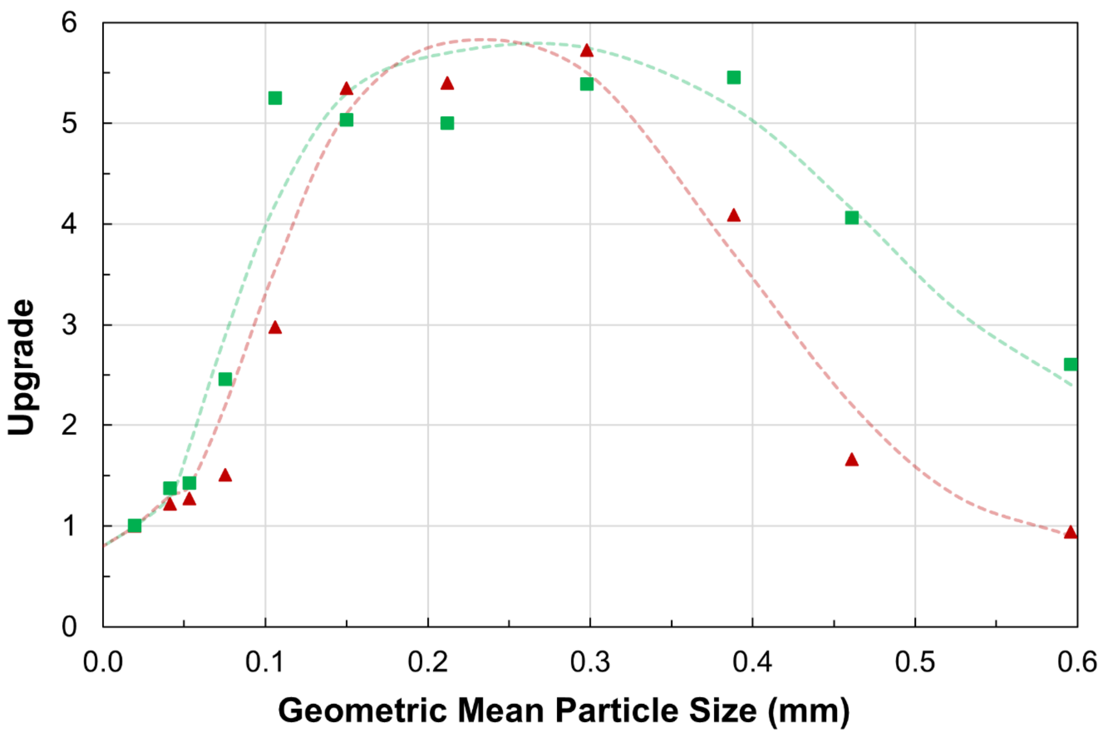

Figure 10. Upgrade, defined as the ratio of product grade to feed grade, as a function of geometric mean particle size for best (green squares) and poorer (red triangles) performing runs. The impact of entrained gangue on the grade of product is shown, where the higher gas flux had a lower associated grade for almost all size intervals.

3.5. Discussion

Copper recovery at fine particle sizes (below 0.090 mm) for the best gas flux case was 99.3 ± 0.3%, while mass rejection was 21 ± 2.8%. This would seem to indicate that there is room for greater mass rejection from the system with minimal impact on copper recovery. However, it remains to be seen whether this is possible at higher solids throughputs. The advantage here is in the practical implications for downstream processing. The overflow product stream in this case contained 40% of the original feed mass, with 50% passing through a screen of an aperture size of 0.038 mm. Classified at 0.038 mm, the undersize would be suitable for conventional flotation in a suitable cleaner arrangement. The oversize from the classifier would require regrinding for further liberation, but only accounts for 20% of the original feed mass, greatly reducing the comminution load. The rejected portion is not reground, reducing energy and water consumption.

It is clear from this work that the recovery of the copper declines as the particle size increases. The chalcopyrite ore undergoes a process of breakage and comminution. Ideally, this comminution leads to the creation of relatively clean fractures and hence formation of high-grade particles that break away from much lower-grade gangue minerals. It is notable that despite the low recovery at the coarsest sizes, the overall recovery was still very strong, suggesting that, in fact, favourable breakage did occur during comminution. This observation is further supported by the very strong upgrade of ~5.5 observed at the intermediate particle size of 0.30 mm, and much lower upgrade at 0.50 mm. Figure 11 shows images of the overflow product, which displays a strong mineral "lustre", and the underflow reject, which displays a dull tone and typically little or no surface liberation. A detailed appraisal of the mineralogy and fracture mechanics of this ore is beyond the scope of this study.

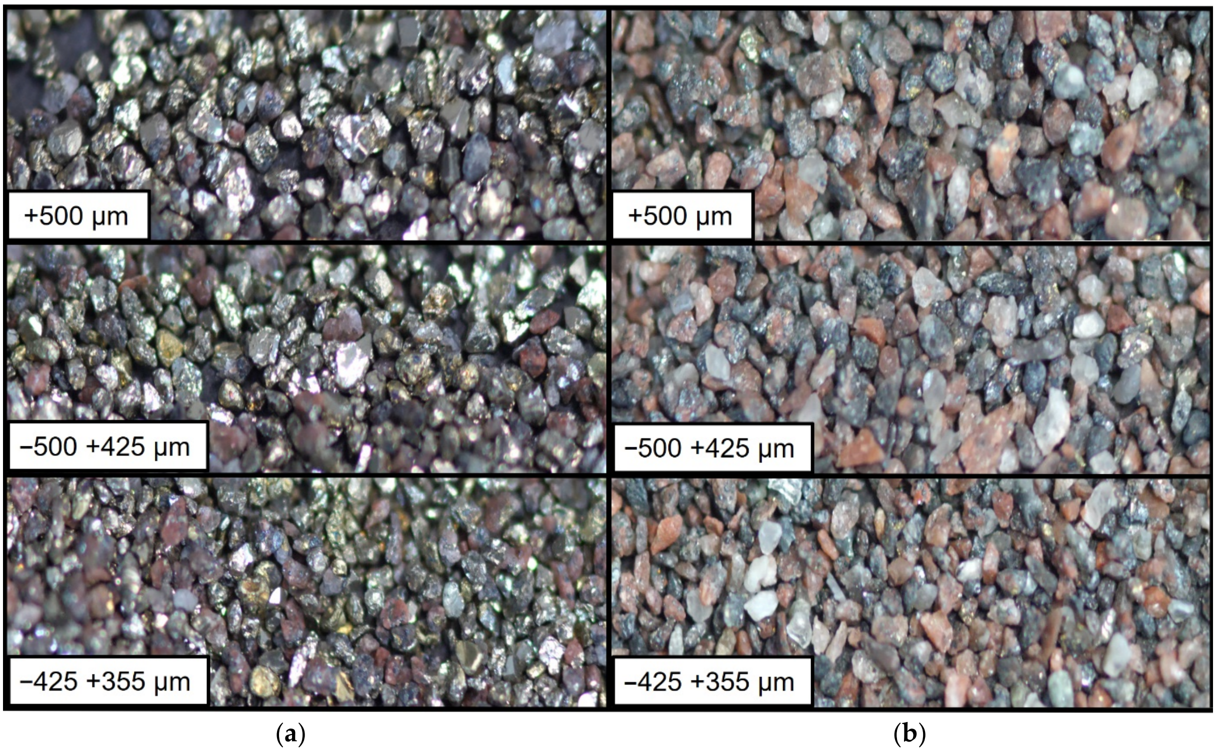

Figure 11. Images of the overflow product (**a**) and underflow reject (**b**) particles show the strong contrast in the surface lustre and hence surface liberation of the particles. Particles were taken from samples collected during Run 2-E (0.3 cm/s gas flux).

What is of greater interest ultimately is the nature of the particles that were not floated in this study. Many of those particles will contain little or no copper, others will contain some copper locked entirely within the surface, and some will contain remnants of copper at the grain boundaries following fracture, but perhaps little else. A smaller portion will likely contain higher levels of copper at the surface that the process failed to recover. Unlike other separation technologies, coarse particle flotation presents significant challenges to both researchers and to industry in forming a rigorous and objective appraisal of the true separation performance. There are two key issues here; the first concerns the hydrodynamic and physicochemical performance of the separator itself, and the second is the value proposition of the separation for the ore in question. We need to develop rigorous answers to the first of these questions before we can begin to properly address the second question, i.e., the value proposition for the industry, which is best answered by deploying the best separator.

Conventional strategies for assessing the performance of the coarse particle flotation commence with bulk measurement of the copper grade, and then consideration of the mineralogy itself. Polished sections again offer insights into the bulk mineralogy of the particles, but also the prospect for inferring surface properties at the perimeter of the particles. X-ray CT scanning has also been used in recent years. These approaches will be valuable from a fundamental perspective but have so far had limited impact in the field. Mineralogy is important, but this must be married hydrodynamically to the performance of the separator. Our group is currently pursuing such an approach, the aim being to assess the separation performance in a manner that is accessible, rigorous, meaningful, and objective.

4. Conclusions

This paper is the first report on the CoarseAIR™. The paper has succeeded in establishing a point of reference on the first critical question concerning internal classification, focusing on the inclined channel spacing and the gas flux. Clear conclusions have been formed. On a real chalcopyrite ore, an overall copper recovery of 90% was achieved, corresponding to a solids gangue rejection of 60%. This performance was achieved using the wider channel spacing of z = 9 mm at a gas flux of 0.15 cm/s. The system performance was robust across the range of conditions investigated.

The new feed protocol has generated high-quality data that adhere consistently to material balance requirements over both short- and long-time scales. The knowledge generated here will inform the next phase of our work. That phase will examine the issue of solids throughput, and the importance of the bed height. If internal classification is to provide value, this will require strong separation performance at much higher solids loadings of between 10 and 20 t/($m^2 \cdot$h).

Author Contributions: L.J.C.: Experiments, Methodology, Writing—original draft, Writing—review and editing, Formal analysis. M.T.I.: Experiments, Methodology, Writing—review and editing. K.P.G.: Experiments, Writing—original draft, Writing—review and editing, Formal analysis, Supervision, Funding acquisition. All authors have read and agreed to the published version of the manuscript.

Funding: The authors acknowledge the funding support from the Australian Research Council for the ARC Centre of Excellence for Enabling Eco-Efficient Beneficiation of Minerals, grant number CE200100009, and other research support from FLSmidth.

Acknowledgments: The contributions of Joshua Sutherland and Matthew Cole to support the running of the experiments, especially in the feed preparation and delivery, and of Isaac De Maria, Jackson Lee, and Tom Maher in sample analysis and feed preparation are gratefully acknowledged.

Conflicts of Interest: The authors acknowledge the University of Newcastle has a Research and Development Agreement with FLSmidth, and IP policy that extends benefits to the inventor, Kevin Galvin.

Appendix A

Table A1. Comparison of raw and mass balanced data for the best and poorer performing sets of experimental conditions. Consistency of the feed composition throughout the experiments delivered strong closure in the material balance, with a requirement of only minor adjustment to experimental values.

Raw Data (Experiment 2C—0.45 cm/s, 9 mm Channels)						
Geometric Mean Size (mm)	**Feed Mass (%)**	**Feed Grade (Cu%)**	**Product Mass (%)**	**Product Grade (Cu%)**	**Reject Mass (%)**	**Reject Grade (Cu%)**
0.596	2.57	0.54	0.12	0.51	4.64	0.54
0.461	4.17	0.59	0.35	0.98	7.15	0.57
0.388	6.80	0.66	0.81	2.64	11.20	0.45
0.298	12.64	0.73	3.10	4.19	19.69	0.28
0.212	11.85	0.85	4.36	4.59	16.67	0.14
0.150	11.17	0.92	4.76	4.92	15.62	0.06
0.106	11.63	0.97	9.14	2.89	15.60	0.03
0.075	8.53	1.03	14.46	1.58	5.44	0.04
0.053	7.09	1.12	12.16	1.40	3.06	0.04
0.041	2.91	1.22	2.89	1.01	0.64	0.05
0.019	20.65	1.35	47.84	1.31	0.28	0.12
Head Grade		0.95		1.67		0.20
Balanced Data (Experiment 2C)						
Geometric Mean Size (mm)	**Feed Mass (%)**	**Feed Grade (Cu%)**	**Product Mass (%)**	**Product Grade (Cu%)**	**Reject Mass (%)**	**Reject Grade (Cu%)**
0.596	2.68	0.54	0.12	0.51	4.88	0.54
0.461	3.94	0.59	0.35	0.98	7.02	0.57
0.388	5.73	0.65	1.08	2.66	9.73	0.46
0.298	12.11	0.73	3.03	4.18	19.94	0.28
0.212	10.92	0.85	3.78	4.59	17.06	0.14
0.150	10.31	0.92	3.96	4.92	15.78	0.06
0.106	12.64	0.97	8.96	2.89	15.80	0.03
0.075	8.81	1.04	12.36	1.57	5.76	0.04
0.053	7.68	1.11	13.01	1.41	3.09	0.04
0.041	1.91	0.96	3.36	1.17	0.66	0.05
0.019	23.28	1.33	50.00	1.33	0.28	0.12
Head Grade		0.97		1.86		0.21
Raw Data (Experiment 2D—0.15 cm/s, 9 mm Channels)						
Geometric Mean Size (mm)	**Feed Mass (%)**	**Feed Grade (Cu%)**	**Product Mass (%)**	**Product Grade (Cu%)**	**Reject Mass (%)**	**Reject Grade (Cu%)**
0.596	2.57	0.56	0.19	1.46	4.37	0.54
0.461	4.17	0.61	0.61	2.49	6.81	0.50
0.388	6.80	0.64	1.41	3.48	11.14	0.40
0.298	12.64	0.72	4.63	3.89	19.26	0.23
0.212	11.85	0.84	5.67	4.19	17.10	0.11
0.150	11.17	0.91	5.68	4.58	15.83	0.05
0.106	11.63	1.00	4.99	5.24	13.43	0.03
0.075	8.53	1.16	8.67	2.86	7.08	0.03
0.053	7.09	1.14	12.10	1.63	3.55	0.03
0.041	2.91	1.18	3.77	1.62	1.03	0.04
0.019	20.65	1.35	52.28	1.37	0.40	0.10
Head Grade		0.95		2.26		0.15

Table A1. *Cont.*

Balanced Data (Experiment 2D)						
Geometric Mean Size (mm)	**Feed Mass (%)**	**Feed Grade (Cu%)**	**Product Mass (%)**	**Product Grade (Cu%)**	**Reject Mass (%)**	**Reject Grade (Cu%)**
0.596	2.67	0.56	0.18	1.46	4.27	0.54
0.461	4.05	0.61	0.59	2.48	6.28	0.50
0.388	6.90	0.64	1.36	3.49	10.47	0.40
0.298	13.27	0.72	4.54	3.88	18.89	0.23
0.212	12.33	0.84	5.61	4.20	16.66	0.11
0.150	12.02	0.91	5.84	4.58	16.01	0.05
0.106	10.68	1.00	5.08	5.25	14.29	0.03
0.075	8.24	1.16	8.45	2.85	8.10	0.03
0.053	6.87	1.14	12.16	1.63	3.46	0.03
0.041	2.54	1.18	4.69	1.62	1.16	0.04
0.019	20.43	1.36	51.51	1.37	0.40	0.10
Head Grade		0.98		2.23		0.17

References

1. Wills, B.A.; Finch, J. *Wills' Mineral Processing Technology: An Introduction to the Practical Aspects of Ore Treatment and Mineral Recovery*; Butterworth-Heinemann: Oxford, UK, 2015.
2. Gaudin, A. Effect of particle size on flotation. *Tech. Publ.* **1931**, *12*, 3–23.
3. Miettinen, T.; Ralston, J.; Fornasiero, D. The limits of fine particle flotation. *Miner. Eng.* **2010**, *23*, 420–437. [CrossRef]
4. Vallejos, P.; Yianatos, J.; Vinnett, L. A Model Structure for Size-by-Liberation Recoveries in Flotation. *Minerals* **2021**, *11*, 194. [CrossRef]
5. Hassanzadeh, A.; Safari, M.; Hoang, D.H.; Khoshdast, H.; Albijanic, B.; Kowalczuk, P.B. Technological assessments on recent developments in fine and coarse particle flotation systems. *Miner. Eng.* **2022**, *180*, 107509. [CrossRef]
6. Goel, S.; Jameson, G.J. Detachment of particles from bubbles in an agitated vessel. *Miner. Eng.* **2012**, *36*, 324–330. [CrossRef]
7. Jameson, G.J. New directions in flotation machine design. *Miner. Eng.* **2010**, *23*, 835–841. [CrossRef]
8. Kohmuench, J.; Luttrell, G.; Mankosa, M. Coarse particle concentration using the HydroFloat Separator. *Min. Metall. Explor.* **2001**, *18*, 61–67. [CrossRef]
9. Napier-Munn, T. Is progress in energy-efficient comminution doomed? *Miner. Eng.* **2015**, *73*, 1–6. [CrossRef]
10. Ballantyne, G.; Powell, M. Benchmarking comminution energy consumption for the processing of copper and gold ores. *Miner. Eng.* **2014**, *65*, 109–114. [CrossRef]
11. Awatey, B.; Skinner, W.; Zanin, M. Incorporating fluidised-bed flotation into a conventional flotation flowsheet: A focus on energy implications of coarse particle recovery. *Powder Technol.* **2015**, *275*, 85–93. [CrossRef]
12. Kohmuench, J.; Mankosa, M.; Thanasekaran, H.; Hobert, A. Improving coarse particle flotation using the HydroFloat™(raising the trunk of the elephant curve). *Miner. Eng.* **2018**, *121*, 137–145. [CrossRef]
13. Awatey, B.; Skinner, W.; Zanin, M. Incorporating a fluidised-bed separator into a conventional flotation set-up. In Proceedings of the Chemeca 2014: Processing Excellence, Powering Our Future, Perth, Australia, 28 September–1 October 2014; pp. 1086–1095.
14. Jameson, G.J.; Emer, C. Coarse chalcopyrite recovery in a universal froth flotation machine. *Miner. Eng.* **2019**, *134*, 118–133. [CrossRef]
15. Boycott, A. Sedimentation of blood corpuscles. *Nature* **1920**, *104*, 532. [CrossRef]
16. Galvin, K.; Zhou, J.; Price, A.; Agrwal, P.; Iveson, S. Single-stage recovery and concentration of mineral sands using a reflux™ classifier. *Miner. Eng.* **2016**, *93*, 32–40. [CrossRef]
17. Galvin, K.; Compton, T.; Firth, B. Quantification of the data improvement produced by optimised metallurgical plant mass balances. *Miner. Eng.* **1995**, *8*, 739–752. [CrossRef]